Cocatalyzing Pt/PtO phase-junction nanodots on hierarchically porous TiO_2 for highly enhanced photocatalytic hydrogen production

ACS APPLIED MATERIALS & INTERFACES

Article

Cocatalysing Pt/PtO Phase-junction nanodots on hierarchically porous TiO2 for highly enhanced photocatalytic hydrogen production

Xiaoning Ren, Zhiyi Hu, Jun Jin, Liang Wu, Chao Wang, Jing Liu, Fu Liu, Min Wu, Yu Li, Gustaaf Van Tendeloo, and Bao-Lian Su

ACS Appl. Mater. Interfaces, **Just Accepted Manuscript** • DOI: 10.1021/acsami.7b07226 • Publication Date (Web): 16 Aug 2017

ACS Publications

ACS Applied Materials & Interfaces is published by the American Chemical Society. 1155 Sixteenth Street N.W., Washington, DC 20036

Cocatalyzing Pt/PtO phase-junction nanodots on hierarchically porous TiO_2 for highly enhanced photocatalytic hydrogen production

Xiao-Ning Ren[a,†], Zhi-Yi Hu[b,†], Jun Jin[a], Liang Wu[a], Chao Wang[a], Jing Liu[a], Fu Liu[c], Min Wu[a], Yu Li*[a], Gustaaf Van Tendeloo[b] and Bao-Lian Su*[, a, d, e]

[a] *Laboratory of Living Materials at the State Key Laboratory of Advanced Technology for Materials Synthesis and Processing, Wuhan University of Technology, 122 Luoshi Road, 430070, Wuhan, Hubei, China;* E-mail addresses: *yu.li@whut.edu.cn and baoliansu@whut.edu.cn*

[b] *EMAT (Electron Microscopy for Materials Science), University of Antwerp, 171 Groenenborgerlaan, B-2020 Antwerp, Belgium*

[c] *School of Materials Science and Engineering, Zhejiang University, 38 Zheda Road, 310027Hangzhou, China*

[d] *Laboratory of Inorganic Materials Chemistry (CMI), University of Namur, 61 rue de Bruxelles, B-5000 Namur, Belgium;* E-mail addresses: *bao-lian.su@unamur.be*

[e] *Clare Hall, University of Cambridge, Cambridge CB21 EW, UK;* E-mail addresses: *bls26@cam.ac.uk*

[†] The authors equally contribute to this work.

* Corresponding authors.

Keywords: Hierarchically meso-macroporous TiO_2; biomolecular self-assembly; cocatalyst; Pt/PtO phase-junction nanodots; photocatalytic H_2 production

Abstract: Phase-junction between cocatalyst and semiconductor host is quite effective to enhance the photocatalytic activity, and is widely studied while the report on the phase-juncted cocatalyst is still rare. In this work, we report the deposition of the Pt/PtO phase-juncted nanodots as cocatalyst via NaOH modification of an interconnected meso-macroporous TiO_2 network with high surface area and inner-particle mesopores to enhance the performance of photocatalytic H_2 production. Our results show that NaOH modification can largely influence the Pt/PtO phase-juncted nanodots formation and dispersity. Comparing to the TiO_2 nanoparticles, the hierarchically meso-macroporous TiO_2 network containing 0.18 wt% Pt/PtO phase-juncted cocatalyst demonstrates the highest photocatalytic H_2 rate of 13 mmol g^{-1} h^{-1} under simulated solar light, and possesses a stable cycling activity without obvious decrease after five cycles. Such high H_2 production performance can be attributed to both phase-juncted Pt/PtO providing more active sites while PtO suppressing the undesirable hydrogen back reaction, and the special hierarchically porous TiO_2 network with inner-particle mesopores presenting short diffusion path lengths for photogenerated electrons and enhanced light harvesting efficiency. This work suggests that Pt/PtO phase-juncted cocatalyst on hierarchically porous TiO_2 nanostructures is a promising strategy for advanced photocatalytic H_2 production.

1. Introduction

Hydrogen has been recognized as a significant clean energy to relieve the increasing energy crisis and environmental contamination caused by the consumption of fossil fuels [1, 2]. Photocatalytic water splitting based on semiconductor photocatalysts is becoming a promising strategy to convert solar energy to clean H_2 fuel [3].

Generally, the photocatalytic activity of a semiconductor is mainly determined by three factors: the photogenerated electron-hole recombination rate, the transfer speed of the photogenerated electrons and the light absorption properties [4, 5]. In the respect of solving photogenerated electron–hole recombination, cocatalysts are often adopted as reaction sites to improve the charge separation and migration at the junctions/interfaces between the cocatalyst and semiconductors [2]. Pt, owing to its large work function, is usually considered as the most suitable H_2 cocatalyst in view of both electronic and catalytic properties to facilitate the interfacial separation of photogenerated electrons and holes [6,7]. Numerous studies have demonstrated that the size and dispersity of Pt on TiO_2 are crucial for the photocatalytic hydrogen production activity [8,9-15]. For example, 5.75 nm Pt nanoparticles have a better H_2 production performance than Pt nanoparticles in sizes of 6 and 6.5 nm [16] although the size difference is very small, indicating that smaller Pt nanoparticles can more effectively restrict the recombination of the photogenerated electrons and holes [15]. A well dispersity of Pt nanoparticles shows an enhanced hydrogen production due to the more active sites to effectively separate the photogenerated charges [17]. Recently, Yang's group found that PtO could also act as an efficient hydrogen evolution site while suppress the undesirable hydrogen back reaction for photocatalytic H_2 production [18]. This finding suggests that the co-existence of Pt and PtO as joint-cocatalyst in photocatalyst with the effect of Pt nanoparticles as separator of

photogenerated charges and the effect of PtO nanoparticles as active sites and suppression of the hydrogen back reaction could be a new way to improve photocatalytic efficiency.[18-21] It should thus be very interesting to have a Pt/PtO phase-junction as cocatalyst to benefit effects of Pt and PtO and also phase-junction phenomenon of Pt/PtO to largely enhance the performance of photocatalytic H_2 production. At present, the phase-junction for photocatalytic activity enhancement however mostly focus on the host photocatalysts. For example, the most popular phase-junction for host photocatalyst is anatase-rutile phase-junction in TiO_2 [22, 23]. The study on the effect in cocatalyst phase-junction such as Pt/PtO nanodots for photocatalytic H_2 production is still rare. On one hand, this finding about PtO as cocatalyst enhancing the photocatalytic activity is very new. On the other hand, it is still lack of a facile strategy to synthesize highly dispersed Pt/PtO cocatalyst in small size [18,19, 24-26].

For the deposition of cocatalyst, the $NaBH_4$ based reduction method is widely adopted for a well dispersity of Pt nanoparticles [18, 27-29]. However, controlling the size of Pt nanoparticles is challenging because the easy hydrolysis property of $NaBH_4$ makes the reduction of metal very fast, resulting in the reaction to a cold water environment. Furthermore, the addition speed and the concentration of $NaBH_4$ are crucial for a well control to prevent inactivation of $NaBH_4$ by restricting the hydrogen evolution when added into water [3, 30-32]. This makes the Pt deposition controls difficult. Recently, Zhai et al. reported that an alkali modification method could suppress the metal particle growth through introduction of alkali-$O_x(OH)_y$ species for well dispersed subnanometer Pt clusters and atoms on alumina or silica, leading to enhanced H_2 production via water-gas shift reaction [33-35]. Thus, the alkali modification of semiconductor host via quickly improving the amounts of the surface bridging hydroxyls could ensure the well dispersity of ultra-small Pt nanoparticles by suppressing the

metal particle growth. Further, the alkali modification can retard the reduction of Pt^{4+} during the Pt deposition.[33-37] In addition, the chemistry of Pt may take place on the atomically dispersed Pt species and involves the nerghboring OH groups on TiO_2 surface, resulting in Pt^0 partially oxidized to Pt^{2+}.[33, 34] This means that alkali modification may introduce Pt^{2+} species in Pt nanoparticles to form Pt/PtO phase-junction.

Herein, we introduce the high dispersity of phase-juncted Pt/PtO hybrid nanodots via a NaOH modification procedure on the hierarchically interconnected meso-macroporous TiO_2 with inner-particle mesopores for largely enhanced photocatalytic H_2 production. In this process, NaOH plays a key role in the formation of Pt^{2+} species by retarding the reduction speed of H_2PtCl_6 and the deposition of highly dispersed Pt/PtO phase-juncted nanodots by modifying the surface of TiO_2.[33,36] In this composite, metallic Pt in the Pt/PtO hybrid nanodots effectively separates the photogenerated electrons and holes, and PtO provides more active hydrogen evolution sites while suppresses the undesirable hydrogen back reaction. The hierarchically meso-macroporous TiO_2 host with high surface area, highly crystalline frameworks and interconnected bicontinuous pores presents not only the opportunity to load highly dispersed phase-juncted Pt/PtO nanodots as cocatalyst for the enhanced photocatalytic H_2 production but also short diffusion paths for photogenerated electrons and multiple scattering of incident light for light harvesting efficiency enhancement owing to the presence of macropores[4,5]. As a result, the as-synthesized hierarchically meso-macroporous TiO_2 with a very low Pt content of 0.18 wt% produces a very high volume of 65 mmol g^{-1} H_2 in 5 hours and exhibits a very stable photocatalytic H_2 production performance.

2. Experimental

2.1 Chemicals and materials

Titanium sulfate, anhydrous methanol, anhydrous ethanol, sodium hydroxide (NaOH), $NaBH_4$ are purchased from Sinopharm Chemical Reagent Ltd. Co. Chloroplatinic acid ($H_2PtCl_6 \cdot 6H_2O$) and Tergitol(TM)XH(nonionic) (P123) is purchased from Sigma Chemical Co. *Lotus pollen* is purchased from Is yuan Gu healthy technology development co., LTD. All the chemicals are used as received.

2.2 Preparation of TiO_2 from Lotus pollen coat (LPC-P-TiO_2)

Lotus pollen (5g) is dispersed in 100 ml anhydrous ethanol. After continuously stirring for 24 h, pollen coat solution with a slight yellow color is obtained. 8g $Ti(SO_4)_2$ is dissolved into 100 ml anhydrous ethanol to produce titania precursor solution. First, 0.4 g P123 is dissolved into the above pollen coat solution (40 ml) followed by the addition of 10 ml titania precursor. After continuous stirring for 2h, another 40 ml distilled water is added into to form reddish brown floccules. The homogeneous mixture is then transferred to Petri dish at room temperature for 12h and then dried at 40 °C in air for 24h. Finally, the black brown powder is calcined in oven at 500 ℃ for 6h to a white powder, which is donated as LPC-P-TiO_2.

2.3 Pt deposition on LPC-P-TiO_2 (LPC-P-TiO_2-Pt)

The LPC-P-TiO_2-Pt catalysts are prepared by impregnation of the above-prepared LPC-P-TiO_2 powders (0.2g) in 20ml of H_2PtCl_6 ($0.05 gml^{-1}$) aqueous solution. After the solution becoming uniform by stirring, 2ml of freshly prepared $NaBH_4$ aqueous solution (2 mg mL^{-1}, containing 0.5 M NaOH) is rapidly added into the solution with vigorous stirring at room temperature. After 2h, another 2ml of freshly prepared $NaBH_4$ aqueous solution (2 mg mL^{-1}, containing 0.5 M NaOH) is injected into the above solution again, keeping stirring for 12h. In the washing process, the precipitate

is washed by deionized water and ethanol for five times, respectively. After being dried at 40°C, the LPC-P-TiO_2-Pt photocatalyst with clean surface is collected. The H_2PtCl_6 aqueous solution with different concentrations from 0.025, 0.05, 0.075 to 0.1 mg ml^{-1} is used. The weight content of Pt is respectively 0.09%, 0.18%, 0.28% and 0.37%, and the samples are labelled as LPC-P-TiO_2-Pt0.09, LPC-P-TiO_2-Pt0.18, LPC-P-TiO_2-Pt0.28 and LPC-P-TiO_2-Pt0.37, respectively.

2.4 Preparation of TiO_2-NPs and TiO_2-NPs-Pt0.18

Titania precursor is first obtained by dissolving 8g $Ti(SO_4)_2$ in 100ml anhydrous ethanol. 10 ml titania precursor is then taken out and dispersed in another 40 ml anhydrous ethanol. After continuous stirring for 2h, 40 ml distilled water is added into the above solution to form a homogeneous mixture, which is further transferred to Petri dish at room temperature for 12h and dried in oven at 50 °C for 24h in air. Finally, the black brown powder is calcined at 500 °C for 6h to obtain TiO_2-NPs. And TiO_2-NPs-Pt0.18 is prepared as the same process for LPC-P-TiO_2-Pt0.18.

2.5 Characterizations

The crystalline structure is conducted by XRD (Bruker D8 Advance diffractometer, Cu Kα radiation, λ=1.54056 Å). The morphology observation is carried out by field emission scanning electron microscopy (FESEM, Hitachi S-4800). Transmission electron microscopy (TEM), high-resolution transmission electron microscopy (HRTEM), scanning transmission electron microscopy-energy dispersive X-ray spectroscopy (STEM-EDX) and high angle annular dark-filed-scanning transmission electron microscopy (HAADF-STEM) are conducted on a Titan 80-300 with double-correctors. A Micromeritics Tristar II 3020 surface area and porosity analyzer is used to obtain the specific surface area and pore-size distribution via the Brunauer-Emmett-Teller (BET) and Barret-Joyner-Halenda (BJH) methods, respectively. A SHIMADZU UV-vis

spectrophotometer is conducted to collect the UV-vis absorption spectra. X-ray photoelectron spectroscopy (XPS, Thermo Fisher ESCALAB 205Xi) is conducted to analyze the surface electronic states of Ti, O and Pt elements. Fluorescence spectrophotometer (Perkin Elmer LS-55) is used to record the photoluminescence (PL) spectra at room temperature with an excitation wavelength at 300 nm with the scanning speed of 500 nm min^{-1}.

2.6 Photocatalytic H_2 production

The glass gas-closed-circulation system with a top irradiation-type reaction vessel is used to perform the photocatalytic H_2-evolution experiment. A PLS-SXE-300C Xe lamp with a UV light density of 34 mW cm^{-2} and visible light density of 158 mW cm^{-2} at a distance of 15 cm is used as simulated solar light. A flow of cooling water is used to maintain the temperature of the reactant solution at 17 $^{\circ}C$ during the test. 20 mg photocatalysts are dispersed in 50 ml water and 30 ml methanol solvent for photocatalytic H_2 evolution, where methanol acted as sacrificial electron donor to capture photogenerated holes during photocatalysis.[36,38,39] The amount of evolved H_2 is monitored by online gas chromatograph (GC 7890A, Agilent) with a thermal conductivity detector (TCD). The AQY (Apparent quantum yields) is evaluated according to the following equation (1) [37]using the same Xe lamp with a 365 nm filter, of which the UV light density is 20 mW cm^{-2}.

$$\begin{aligned} AQY &= \frac{\text{Number of reacted electrons}}{\text{Number of incident photons}} \times 100\% \\ &= \frac{\text{Number of evolved } H_2 \text{ molecules} \times 2}{\text{Number of incident photons}} \times 100\% \end{aligned} \quad (1)$$

3. Results and discussion

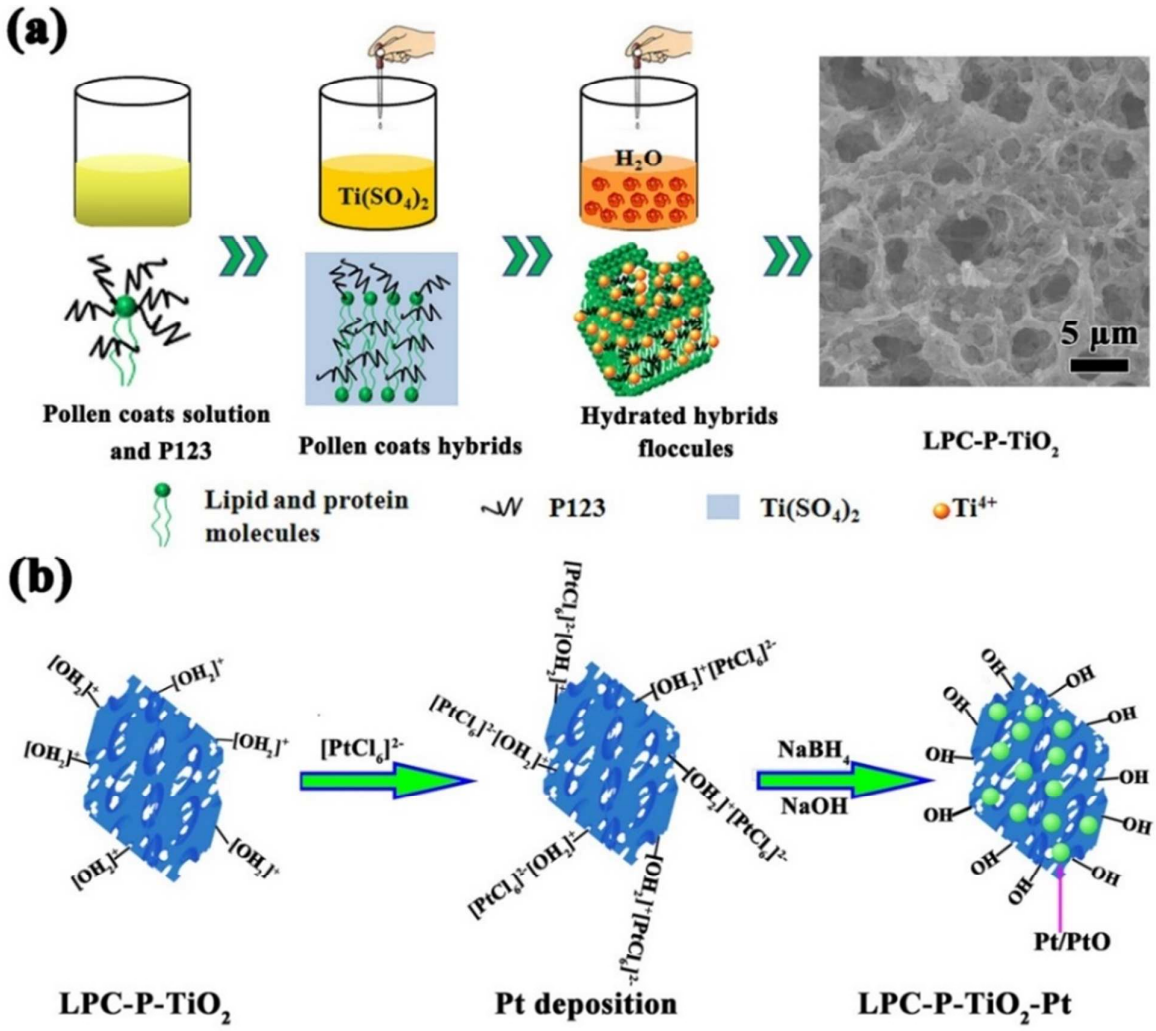

Figure 1. (a) Schematic synthesis process of LPC-P-TiO_2 and (b) phase-juncted Pt/PtO hybrid nanodots formation via NaOH modification of LPC-P-TiO_2.

First, hierarchically porous TiO_2 with inner-particle mesopores via the mediation of the lipids and proteins biomolecular self-assembly from *lotus pollen coat* (LPC) is prepared and selected as the host photocatalyst (donated as LPC-P-TiO_2) [40]. Figure 1a illustrates the preparation process of LPC-P-TiO_2, where LPC acts as a biotemplate for the formation of macropores and P123 is a soft-template for the generation of inner-particle mesopores [41]. The organic groups (mainly hydroxyls) in LPC have intention to interact with metal ions and thus lead to TiO_2 nanocrystallites selective

growth in the framework. The hydrophilic polyethylene oxide in P123 interacts with the hydrophilic polar ionic groups in LPC. After removal of the templates by calcination, the hierarchially meso-macroporous TiO_2 is obtained. The SEM image clearly shows the hierarchically porous TiO_2 structure (Figure 1a inset).

Figure 1b displays the process of NaOH modification accompanying with the deposition of phase-juncted Pt/PtO hybrid nanodots on the as-prepared hierarchically porous TiO_2. During this process, $PtCl_6^{2-}$ is firstly combined with OH^- on the surface of TiO_2 [42], which guarantees the tightly attachment of $PtCl_6^{2-}$ on the surface of TiO_2. Furthermore, the surface modification of TiO_2 surface by the addition of NaOH increases the surface bridging hydroxyls [43] to provide more active sites for $PtCl_6^{2-}$ anchoring on TiO_2. This helps for the highly dispersity of ultra-small Pt/PtO hybrid nanodots. In addition, NaOH in the solution retards the reduction speed of H_2PtCl_6 during the Pt deposition at room temperature [33, 36], leading to the formation of phase-juncted Pt/PtO hybrid nanodots as cocatalyst.

Figure 2a presents the XRD patterns of the as-prepared samples before and after Pt deposition. It shows that with Pt/PtO deposition, all samples display only anatase TiO_2 phase, indicating the highly dispersed Pt/PtO hybrid nanodots in very small size. Figure 2b compares the FT-IR spectra of LPC-P-TiO_2 and LPC-P-TiO_2-Pt0.18. It shows that after Pt loading, the intensity of the TiO_2 peaks is enhanced. Note that three new peaks at the range of 1200-1600 cm^{-1} appear after Pt/PtO deposition. According to the following Raman results, these peaks should mainly result from the Pt–O–Pt bond. Figure 2c further displays the Raman spectra of LPC-P-TiO_2 and LPC-P-TiO_2-Pt0.18. The peaks at 144, 197, 399, 639 and 519 cm^{-1} correspond to the characteristics of TiO_2 [44]. In particular, there is a peak at around 360-382 cm^{-1} for LPC-P-TiO_2-Pt0.18 (Figure 2d), indicating the existence of Pt-O-Pt

in the sample [45]. These results suggest that the TiO_2 surface modification by the addition of NaOH during the reduction of H_2PtCl_6 via $NaBH_4$ at room temperature can introduce the Pt^{2+} species to form Pt/PtO phase-juncted nandots, consistent with the following XPS result. The existence of PtO may also stabilize the Pt/PtO cocatalyst via tightly anchoring on host TiO_2, leading to the high stability of H_2 production.

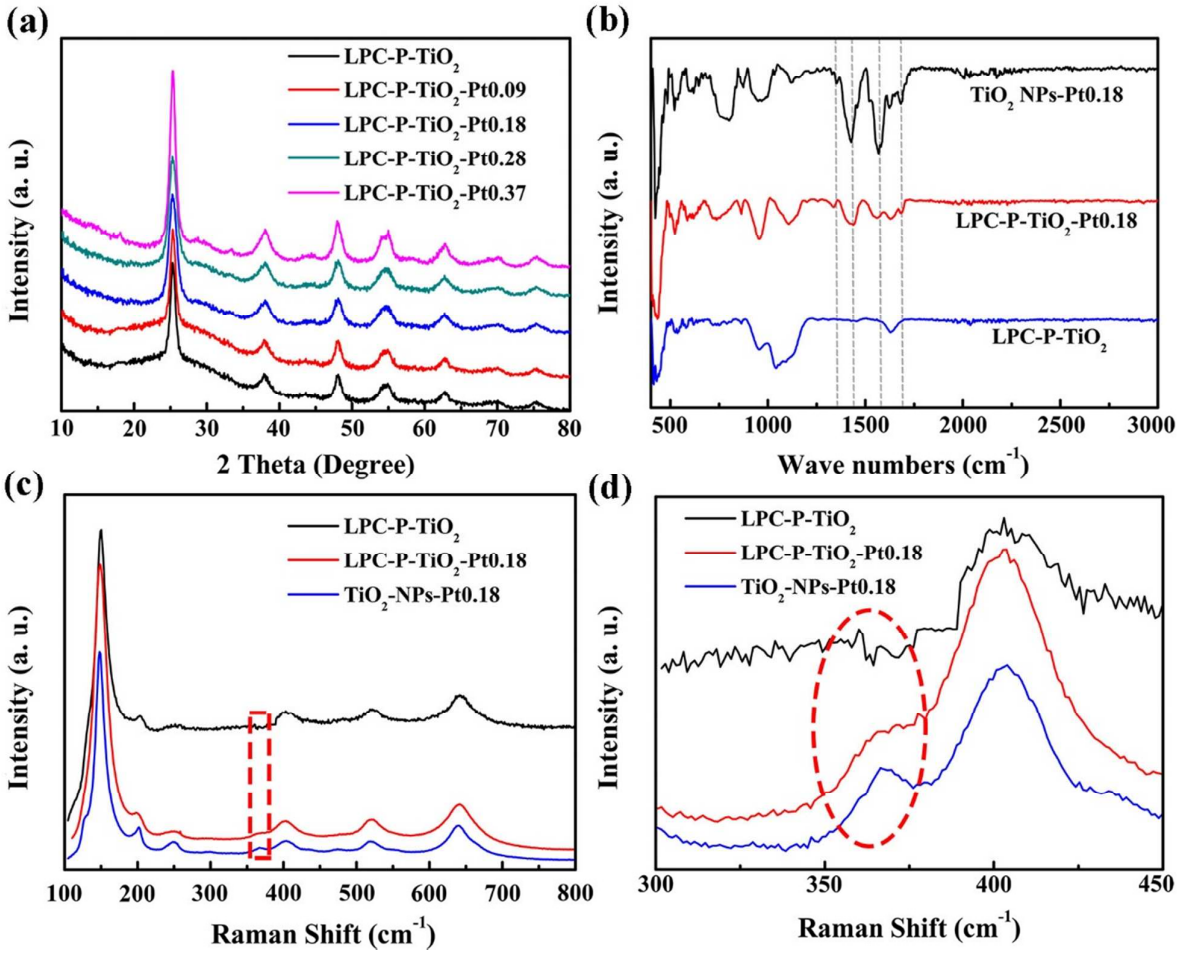

Figure 2. (a) XRD patterns of LPC-P-TiO_2 and LPC-P-TiO_2 with different Pt deposition, (b) FT-IR spectra of LPC-P-TiO_2, LPC-P-TiO_2-Pt0.18 and TiO_2-NPs-Pt0.18, (c) Raman spectra of LPC-P-TiO_2, LPC-P-TiO_2-Pt0.18 and TiO_2-NPs-Pt0.18, (d) the enlarged squared area of the region 300-450 cm^{-1} in (c).

XPS measurements are then carried out to reveal more chemical information for the samples with or without Pt deposition. Figure 3a shows the survey spectra of LPC-P-TiO_2,

LPC-P-TiO_2-Pt0.18 and LPC-P-TiO_2-Pt0.37. The peaks of Ti and O can be clearly observed. It is interesting to note that there is no peak of C for LPC-P-TiO_2. However, both LPC-P-TiO_2-Pt0.18 and LPC-P-TiO_2-Pt0.37 demonstrate peak of C. Most possibly, the existence of C comes from the adsorption of CO_2 in air. In addition, the intensity of C peak from LPC-P-TiO_2-Pt0.18 is higher than that of LPC-P-TiO_2-Pt0.37, indicating more active sites in LPC-P-TiO_2-Pt0.18. Figure 3b demonstrates the Ti2p spectra. The peaks located at 464.5 and 458.8 eV with a peak separation of 5.7 eV are indicative of a Ti^{4+} oxidation state [46, 47]. The O1s spectra can be divided into three peaks (Figure 3c): the peak at 530.3 eV corresponds to Ti-O, the peak at 533.2 eV is from O-H and the peak at 531.5 eV is from oxygen-deficient regions [32]. Figure 3d shows the Pt4f spectra of LPC-P-TiO_2-Pt0.18 and LPC-P-TiO_2-Pt0.37. It clearly displays that LPC-P-TiO_2-Pt0.18 has four peaks at 70.8, 72.7, 74.2 and 76.1 eV for Pt 4f. The peaks at 70.8 and 72.7 eV correspond to metallic Pt^0 states of Pt $4f_{7/2}$ and Pt $4f_{5/2}$, respectively. The main peaks of Pt $4f_{7/2}$ and Pt $4f_{5/2}$ centering at 72.7 and 76.1 eV can be assigned to Pt^{2+} bonded to oxygen, respectively, confirming the coexistence of metallic Pt^0 and oxidized Pt^{2+} [9,18,19]. This verifies that the surface modification of TiO_2 by NaOH can bring Pt^{2+} species in Pt nanoparticles. Note that there is no Pt signal for LPC-P-TiO_2-Pt0.09, we argue that this is due to the very low content of Pt inside this sample. However, LPC-P-TiO_2-Pt0.28 and LPC-P-TiO_2-Pt0.37 only demonstrate two peaks at 70.8 and 74.2 eV (Figure 3d). The absence of the peaks at 72.7 and 76.1 eV indicates no Pt^{2+} species existing in these two samples. This suggests that NaOH can only retard the reduction of H_2PtCl_6 at a low content. This is possible because at the high concentration of H_2PtCl_6, the nucleation speed of Pt nanocrystallites is faster than that at the low concentration. The numbers of Pt nanocrystallites at high concentration are also larger than those at low concentration. However, the XPS results on O 1s and Ti 2p in three samples are quite similar,

indicating no conspicuous affection occurring on the surface atomic structures of the host TiO_2 and Pt/PtO hybrid nanodots. This is consistent with the previous FT-IR and Raman analysis concerning the presence of Pt-O-Pt species only in LPC-P-TiO_2-Pt0.18. Thus, the metallic Pt^0 species attached on the TiO_2 surface, acting as cocatalyst, can serve as the active sites trapping photogenerated electrons and facilitating the H_2 production. The oxidized Pt^{2+} species in Pt/PtO hybrid nanodots acting as photocatalytic activity sites on one hand, can promote the hydrogen production, and on the other hand suppress the hydrogen back reaction in the photocatalytic water splitting [18,19], resulting in a highly enhanced capability for hydrogen production.

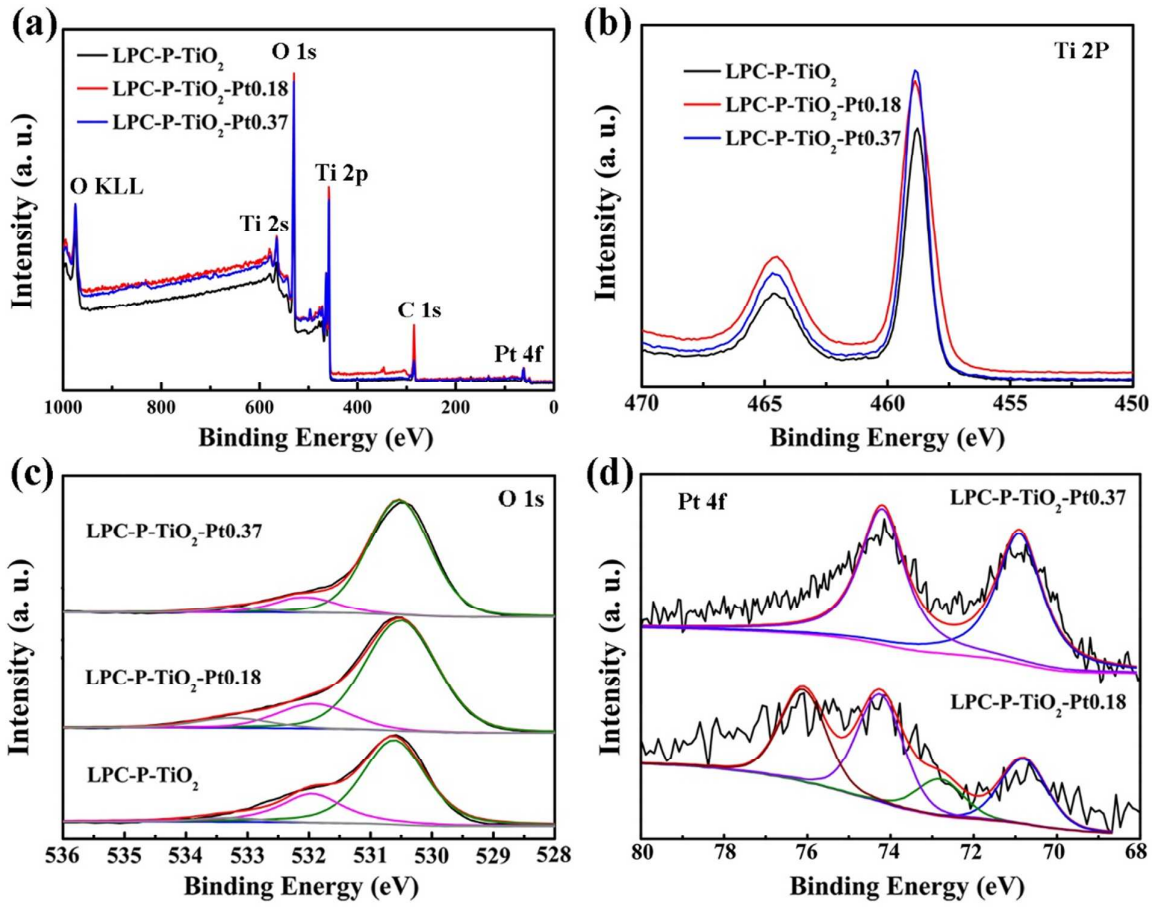

Figure 3. (a) Survey scan XPS spectrum and high resolution XPS spectra of (b) Ti 2p, (c) O 1s peaks of LPC-P-TiO_2, LPC-P-TiO_2-Pt0.18 and LPC-P-TiO_2-Pt0.37, (d) Pt 4f peaks of LPC-P-TiO_2-Pt0.18 and LPC-P-TiO_2-Pt0.37.

Figure 4a presents a typical SEM image of LPC-P-TiO_2-Pt0.18. The average size of the interconnected macropores is ~200 nm. Figure 4b clearly reveals that the framework of LPC-P-TiO_2-Pt0.18 is constructed by many aggregated TiO_2 nanoparticles, forming the interconnected hierarchically meso-macroporous flake-like structure. Figure 4c presents a low magnification TEM image, showing that the TiO_2 nanoparticles are tightly aggregate to form inner-particle mesopores in the interconnected macroporous framework. The TiO_2 nanoparticles have an average size of 8 nm, providing short path lengths for photogenerated charges transfer. The HRTEM image (Figure 4d) clearly demonstrates the inner-particle mesopores (~2 nm in size) and well dispersed Pt/PtO hybrid nanodots (red circled). The inserted fast Fourier transform (FFT) in Figure 4d shows the (101) and (004) crystal rings of TiO_2.

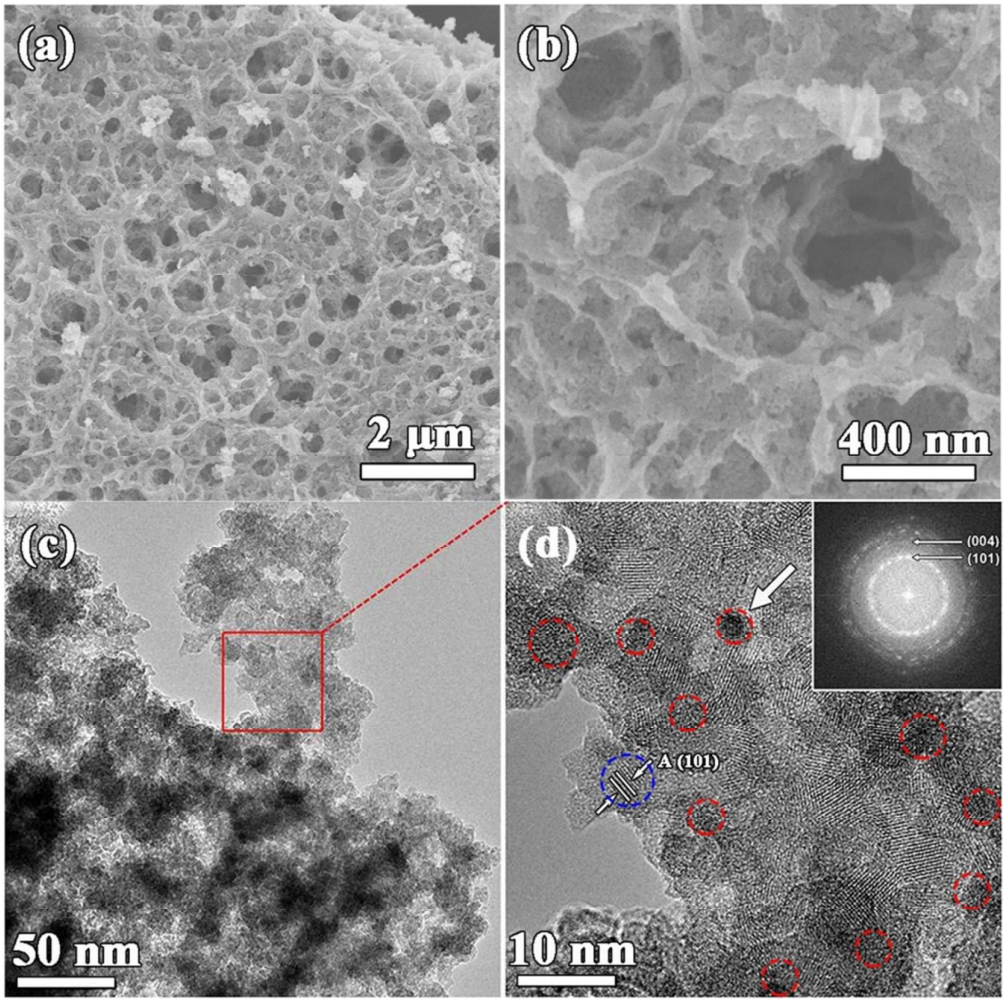

Figure 4. (a-b) SEM images and (c) TEM and (d) HRTEM images of LPC-P-TiO_2-Pt0.18. Pt/PtO nanodots are indicated by red circles and the inset FFT is from the whole area of (d).

To clearly show the distribution of the phase-juncted Pt/PtO hybrid nanodots in such hierarchically meso-macroporous TiO_2 structure, the analysis on elemental distribution in LPC-P-TiO_2-Pt0.18 is further carried out by EDX. Figure 5a-b present the typical HAADF-STEM images, revealing the high dispersity and small size of the Pt/PtO hybrid nanodots. It displays that the Pt/PtO hybrid nanodots are attached on the hierarchically macro-mesoporous TiO_2. From the corresponding HRTEM image, well dispersed Pt/PtO hybrid nanodots with the average size of ~2.5 nm can be clearly observed (Figure 5c). Through our intensive STEM observation, Pt and PtO in the Pt/PtO nanodots is not distinguishable. Most possibly, the PtO and Pt are well mixed in the phase-juncted Pt/PtO hybrid nanodots [18,19, 36]. The STEM-EDX maps of Ti and Pt shown in Figure 5d-f are from the same area shown in Figure 5b. The results confirm that the meso-macroporous TiO_2 structure with inner-mesoporosity is beneficial for ultra-small Pt/PtO hybrid nanodots deposition and dispersity. Upon our intensive TEM observation, the average size of Pt/PtO nanodots in LPC-P-TiO_2-Pt0.09 is at ~2.4nm, and the average size of Pt nanodots in LPC-P-TiO_2-Pt0.28 and LPC-P-TiO_2-Pt0.37 is at ~2.5 and ~2.6 nm, respectively, very close to the size of Pt/PtO nanodots in LPC-P-TiO_2-Pt0.18.

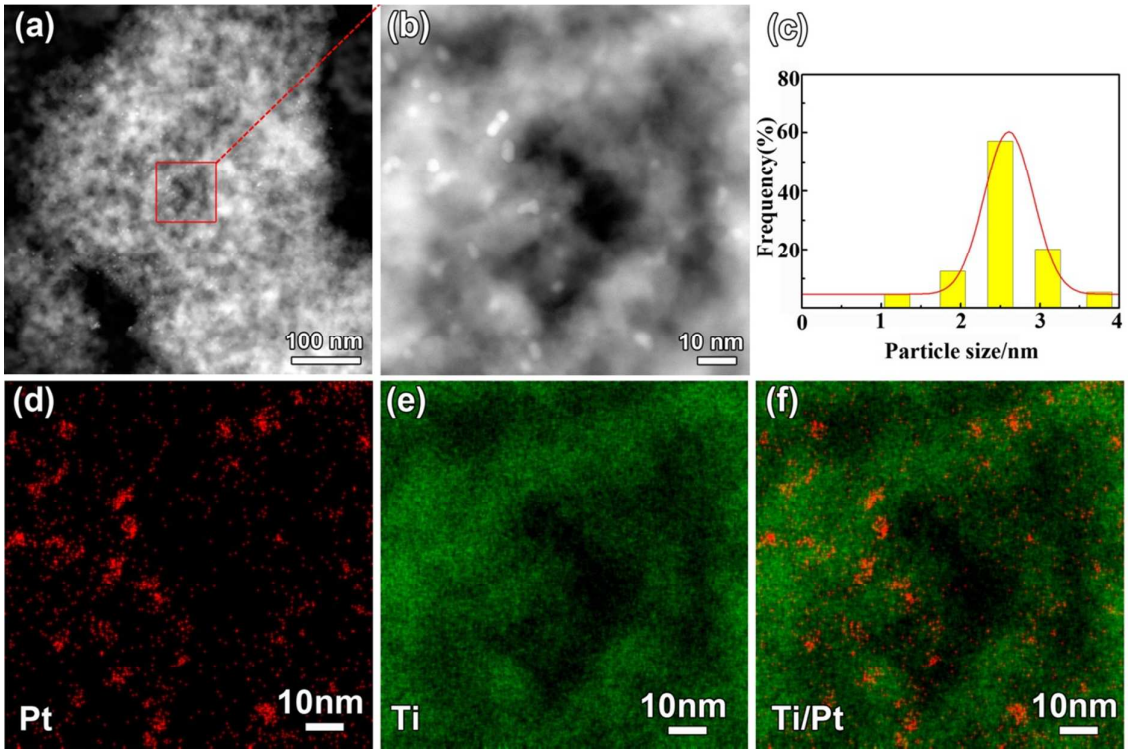

Figure 5. (a) Low magnification HAADF-STEM image of LPC-P-TiO_2-Pt0.18, (b) corresponding high magnification HAADF-STEM image indicated by a red box in (a), (c) Pt nanodot size calculated from the HAADF-STEM images and (d-f) corresponding EDX elemental maps (Pt: red, Ti: green).

To verify the inner-particle mesopores structural stability, the N_2 adsorption-desorption is conducted on the LPC-P-TiO_2 and LPC-P-TiO_2-Pt samples. Figure 6a presents the N_2 isotherms with a H3 hystersis loop, indicating the presence of mesoporous structure. All the samples have a similar pore size distribution at ~2 nm (Figure 6b), in agreement with the HRTEM images. Table 1 lists the obtained data. The result shows that after NaOH modification accompanying with the phase-juncted Pt/PtO hybrid nanodots deposition, all the specific surface areas of the LPC-P-TiO_2-Pt samples increase a little, verifying that the alkali modification of TiO_2 can introduce more active sites for Pt/PtO deposition. However, the pore size distribution is still unchanged, indicating the very stable inner-particle mesoporous structure. Therefore, such a stable hierarchically porous TiO_2 network

with high specific surface area, low density and stable inner-particle mesopores can act as efficient light harvestor to offer a short path length and a bicontinuous transport path for light diffusion. This ensures an enhanced incident light utilization and a relatively high performance for photocatalytic H_2 production.

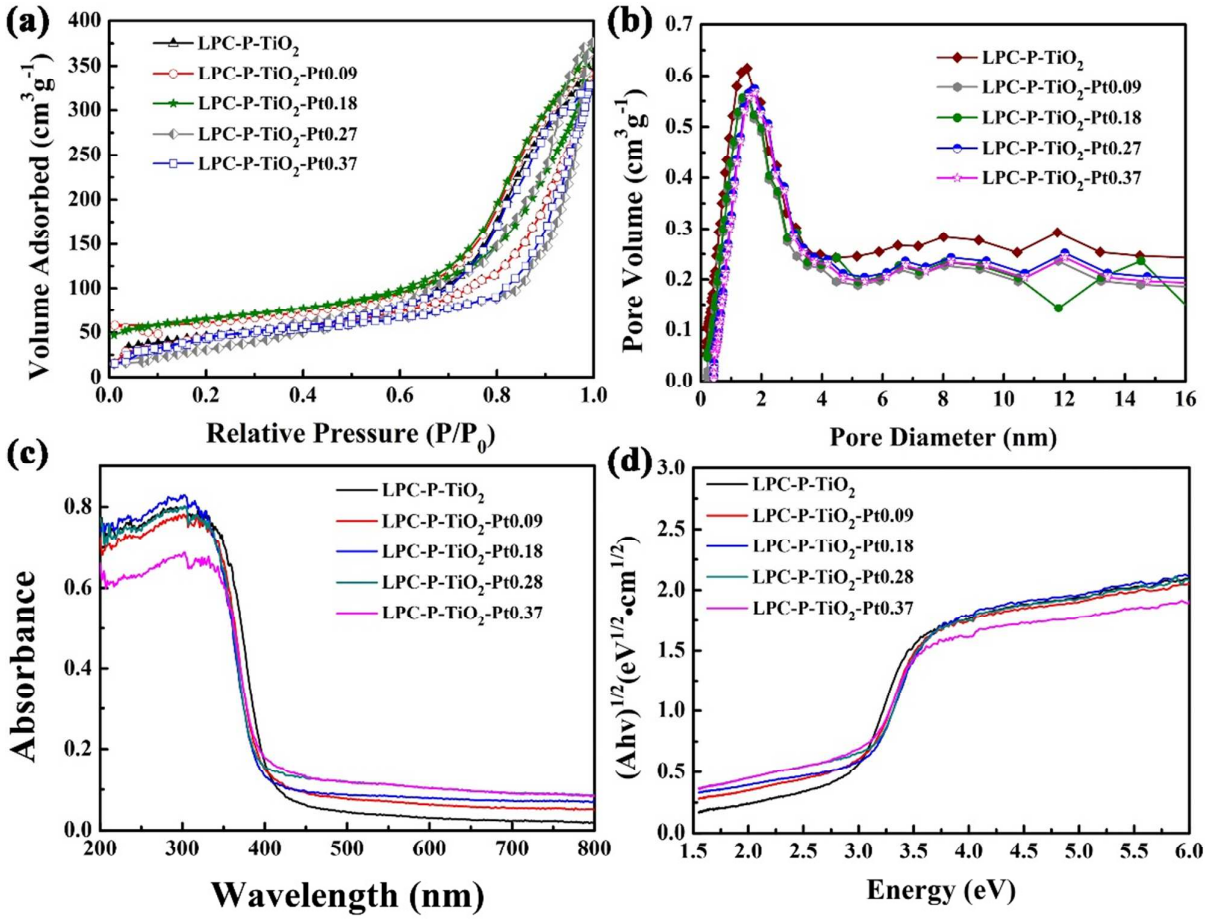

Figure 6. (a) N_2 adsorption-desorption isotherms and (b) the corresponding BJH pore size distribution plot of LPC-P-TiO_2 and LPC-P-TiO_2-Pt samples. (c) UV-vis absorption spectra and (d) the corresponding Tauc plot $(ahv)^{1/2}$ versus the energy (hν) for the band gap energies of LPC-P-TiO_2 and LPC-P-TiO_2-Pt samples.

Figure 6c shows the UV-Vis absorption spectra of LPC-P-TiO_2 and LPC-P-TiO_2-Pt. A significant increase in the absorption at wavelengths shorter than 400 nm can be assigned to the intrinsic band gap absorption of anatase TiO_2. Typically, a Tauc plot shows the quantity *hv* (the

energy of the light) on the abscissa and the quantity $(ahv)^{1/2}$ on the ordinate, where *a* is the absorption coefficient of the material (Figure 6d). Compared to the original LPC-P-TiO_2, the LPC-P-TiO_2-Pt shows a little blue-shift on absorption spectra, due to the interaction between Pt or Pt/PtO nanoclusters and TiO_2. All the obtained electronic energy band gaps (E_g) from the intercept of the tangents are listed in Table 1. In particular, the electronic energy band gap of LPC-P-TiO_2-Pt0.18 shows the largest blue-shift due to the formation of Pt-O-Pt bonds in Pt/PtO nanodots. However, the low content of Pt/PtO nanodots in LPC-P-TiO_2-Pt0.09 leads to weak interaction between Pt/PtO nanodots and TiO_2, indicating that the photocatalytic performance of LPC-P-TiO_2-Pt0.09 is lower than that of LPC-P-TiO_2-Pt0.18.

Table 1 Structure, band gaps, specific surface areas and pore sizes of the samples

Sample	Pt or Pt/PtO size (nm)	Eg (eV)	S_{BET} (m^2g^{-1})	Pore Diameter (nm)
LPC-P-TiO_2	NA	2.85	156	2
LPC-P-TiO_2-Pt0.09	~2.4	2.91	163	2
LPC-P-TiO_2-Pt0.18	~2.5	2.92	168	2
LPC-P-TiO_2-Pt0.27	~2.5	2.92	165	2
LPC-P-TiO_2-Pt0.37	~2.6	2.91	164	2
TiO_2-NPs	NA	3.00	6	NA
TiO_2-NPs-Pt0.18	~3.5	3.00	7	NA

*NA indicates no data.

To further show the advantages of this unique hierarchical meso-macroporous TiO_2 structure for Pt/PtO phase-junction deposition and dispersity, TiO_2 nanoparticles (TiO_2-NPs) in size of ~18 nm is also prepared. The Pt deposition process is the same as the preparation of LPC-P-TiO_2-Pt. The FT-IR and Raman characterizations are displayed in Figure 2b-d, showing the successful deposition of the phase-juncted Pt/PtO hybrid nanodots on TiO_2-NPs. Figure 7a provides the HRTEM image of TiO_2-NPs after loading 0.18 wt% Pt (donated as TiO_2-NPs-Pt0.18). It shows that the dispersity of

Pt/PtO hybrid nanodots is not as good as that on LPC-P-TiO_2-Pt0.18. Many Pt/PtO hybrid nanodots aggregate together. In addition, the mean size of Pt/PtO hybrid nanodots on TiO_2-NPs-Pt0.18 is at ~3.5 nm (Figure 7b), which is much larger than that on LPC-P-TiO_2-Pt0.18. This further confirms that the hierarchically meso-macroporous TiO_2 structure is beneficial for Pt/PtO deposition and dispersity.

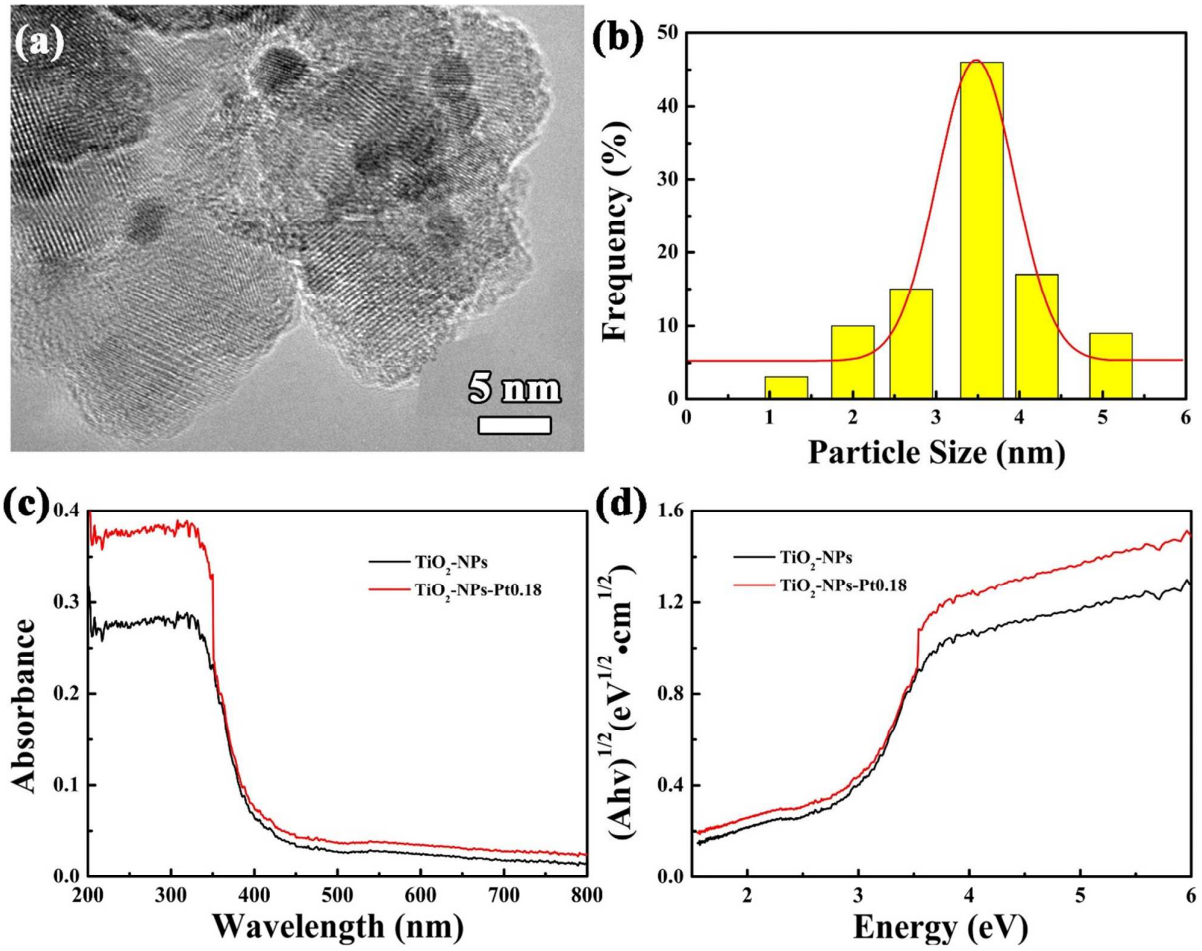

Figure 7. (a) HRTEM images of TiO_2-NPs-Pt0.18, (b) Pt/PtO nanodot size distribution calculated from the HAADF-STEM images, (c) UV-vis absorption spectra and (d) the corresponding Tauc plot $(ahν)^{1/2}$ versus the energy (hν) for the band gap energies of TiO_2-NPs and TiO_2-NPs-Pt0.18.

The UV-Vis absorption is also carried out on TiO_2-NPs and TiO_2-NPs-Pt0.18 as shown in Figure 7c and 7d. From the UV-Vis absorption spectra and Table 1, one can see that there is no obvious change on electronic energy band gap for TiO_2-NPs before and after Pt/PtO deposition. This

indicates that the NaOH modification of TiO_2-NPs cannot introduce enough amounts of hydroxyls to modulate Pt deposition because of the very low surface area (Table 1). This can also explain the Pt/PtO hybrid nanodots aggregation on TiO_2-NPs comparing to the well dispersed Pt/PtO hybrid nanodots on LPC-P-TiO_2-Pt0.18.

The hierarchically interconnected meso-macroporous LPC-P-TiO_2-Pt samples are then used for H_2 evolution under simulated solar light. The H_2 production for the as-prepared TiO_2-NPs and LPC-P-TiO_2 without Pt/PtO nanodots is also conducted. The hydrogen production amount of TiO_2-NPs and LPC-P-TiO_2 in five hours is 0.105 mmol g^{-1} and 0.326 mmol g^{-1}, respectively, which is far worse than that of the LPC-P-TiO_2-Pt samples (Figure 8a). As can be seen, the Pt content has a significant influence on the photocatalytic activity of LPC-P-TiO_2-Pt. The LPC-P-TiO_2-Pt0.18 with a Pt content of 0.18 wt% achieves the highest hydrogen production of 65 mmol g^{-1} in 5 hours. For LPC-P-TiO_2-Pt0.09, its photocatalytic activity is the lowest among these samples. This should be attributed to the very low Pt content because there is no signal of Pt for XPS characterization. Although the Pt content in LPC-P-TiO_2-Pt0.28 and LPC-P-TiO_2-Pt0.37 is high, their photocatalytic activities are similar and much lower than that of LPC-P-TiO_2-Pt0.18. This means that high content of Pt in TiO_2 is not helpful for the enhancement of photocatalytic activity, similar to the previous work [48]. Note that the size of Pt nanodots in LPC-P-TiO_2-Pt0.28 and LPC-P-TiO_2-Pt0.37 is very close to that of Pt/PtO nanodots in LPC-P-TiO_2-Pt0.18. Therefore, the high photocatalytic activity of LPC-P-TiO_2-Pt0.18 comes from the Pt/PtO phase-junction in TiO_2. On one hand, Pt in the phase-juncted Pt/PtO hybrid nanodots effectively separates the photogenerated electrons and holes [49]. On the other hand, PtO in the phase-juncted Pt/PtO hybrid nanodots provides more active hydrogen evolution sites as well as suppresses the undesirable hydrogen back reaction [9,18,19]. The phase junction

formed between Pt and PtO can be also beneficial for the improved separation of photogenerated electrons and holes and help the migration of charges. Figure 8a also displays the H_2 production of TiO_2-NPs-Pt0.18. Due to the larger Pt/PtO hybrid nanodots and their aggregation, its H_2 production performance is just a little better than that of LPC-P-TiO_2-Pt0.09. This also suggests that the size and dispersity of Pt/PtO is crucial for photocatalytic H_2 production.

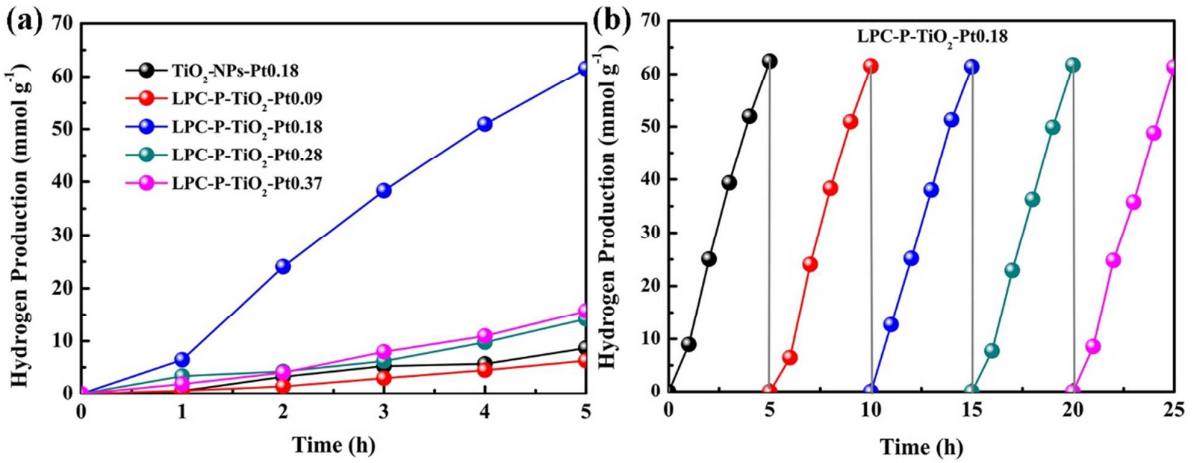

Figure 8. (a) H_2 production performance of LPC-P-TiO_2-Pt with different amounts of Pt and TiO_2-NPs-Pt0.18, (b) the cycling performance of LPC-P-TiO_2-Pt0.18.

The hydrogen production performance under a monochromatic light of 365 nm is 21.27 mmol g^{-1}, which is almost 1/3 comparing to the production under full light spectrum. The hydrogen production rate is 0.085 mmol h^{-1}, and the AQY is 77.48% according to the equation (1). The stability of LPC-P-TiO_2-Pt0.18 for H_2 production is further investigated. Figure 8b displays the cycling performance. It shows that after 5 cycles for 25 hours, the H_2 production still keeps at ~65 mmol g^{-1}, demonstrating a very high stability and sustainability. This is very helpful for practice utilization.

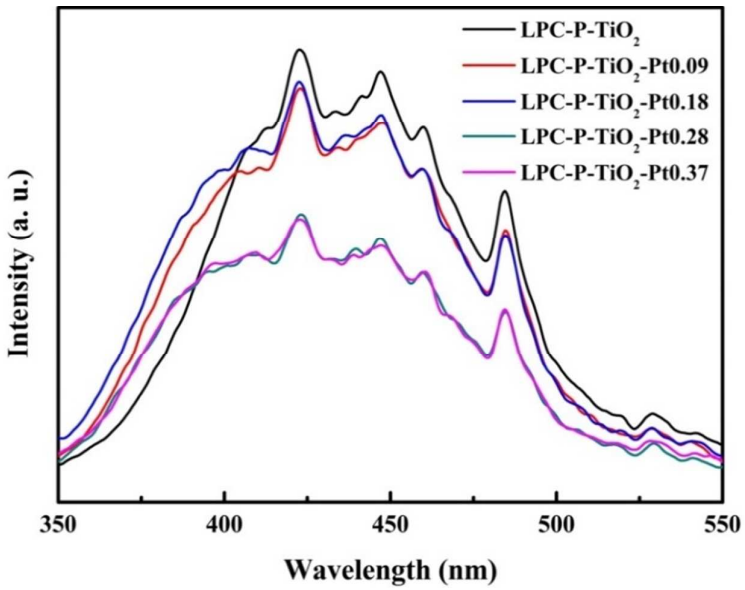

Figure 9. PL spectra of LPC-P-TiO_2 and LPC-P-TiO_2 with varies Pt deposition.

Photoluminescence (PL) emission spectrum is then used to investigate the efficiency of photogenerated electrons and holes separation and immigration. Figure 9 shows the PL spectra of LPC-P-TiO_2 and LPC-P-TiO_2-Pt in the wavelength range of 350-550 nm. The PL spectrum of LPC-P-TiO_2 is similar to those of LPC-P-TiO_2-Pt. The emission peak at ~420 nm is approximately equal to the electronic energy band gaps of the samples, consistent with the UV-Vis analysis (Table 1). The PL peaks at around 451 and 468 nm are contributed to band edge free excitation. The small peaks in the wavelength range of 480-550 nm are mainly resulted from defects of the synthesized TiO_2 [14, 50-52]. It can be seen that LPC-P-TiO_2 displays higher peak intensity compared to the LPC-P-TiO_2-Pt samples, implying a higher recombination rate of photogenerated electrons and holes under UV light irradiation. Both LPC-P-TiO_2-Pt0.28 and LPC-P-TiO_2-Pt0.37 demonstrate lower intensity comparing to LPC-P-TiO_2-Pt0.09 and LPC-P-TiO_2-Pt0.18, suggesting an efficient separation of photogenerated electrons and holes, which can result in a good H_2 production. However, the experimental result shows that LPC-P-TiO_2-Pt0.18 has the best performance for H_2 production.

From the results and analysis above, it can be concluded that it is the Pt/PtO phase-junction in the samples that greatly influences the final performance for photocatalytic H_2 production. Namely, although the combination rate of photogenerated electrons and holes of LPC-P-TiO_2-Pt0.18 is higher than those of LPC-P-TiO_2-Pt0.28 and LPC-P-TiO_2-Pt0.37, the phase-juncted Pt/PtO hybrid nanodots as cocatalyst in LPC-P-TiO_2-Pt0.18 can largely compensate the negative effect of fast combination of photogenerated electrons and holes, leading to the enhanced photocatalytic activity for H_2 production. In other words, the Pt/PtO phase-junction cocatalyst can improve the utilization of the photogenerated electrons. More detailed work should be carried out to verify this. As for LPC-P-TiO_2-Pt0.09, the low Pt content should limit its final performance, indicating that enough Pt content is necessary.

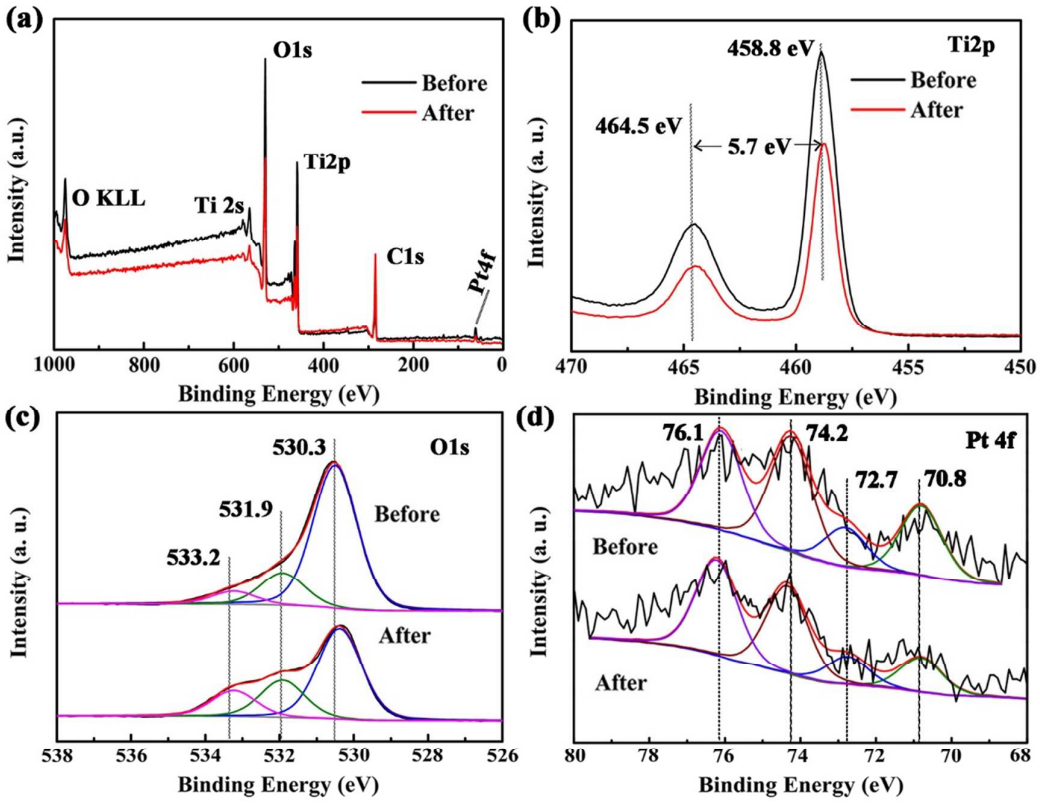

Figure 10. (a) Survey scan XPS spectrum and high resolution XPS spectra of (b) Ti 2p, (c) O 1s peaks and (d) Pt 4f peaks of LPC-P-TiO_2-Pt0.18 before and after photocatalytic H_2 production.

XPS measurements are again carried out to reveal chemical information on the reacted LPC-P-TiO_2-Pt0.18 photocatalyst after 5 cycles (Figure 10). It shows that after the reaction, the spectra on O 1s and Ti 2p are quite similar to the original spectra, indicating no detective affection on the surface atomic structures of the host TiO_2 and the cocatalyst Pt/PtO hybrid nanodots after reaction. Still, four peaks of Pt4f at 70.8, 72.7, 74.2 and 76.1 eV exist after cycled reaction. Specifically, the intensity of the O-H peak at 533.2 eV is a little enhanced after the photocatalytic reaction (Figure 10c), indicating an increased amounts of the surface hydroxyl, which is helpful to enhance the hydrogen production performance by accelerating the electron transportation via modulating the electronic energy band gap [33, 41], and is also beneficial for LPC-P-TiO_2-Pt0.18 to keep its stability for the photocatalytic H_2 production.

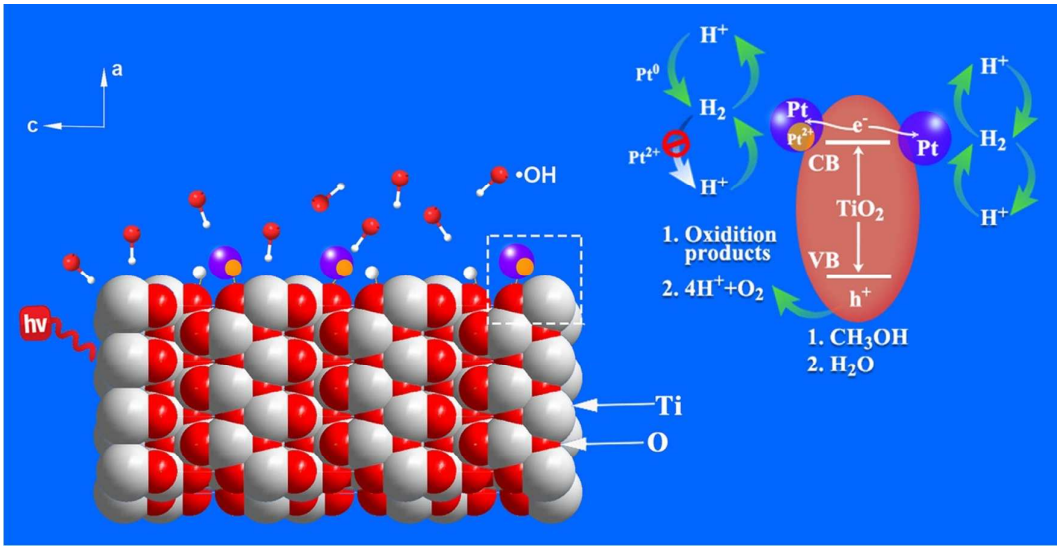

Figure 11. Shematic diagram of the mechanism of the Pt/PtO phase-junction hybrid nanodots on TiO_2 (001) plane for photocatalytic H_2 production under simulated solar light.

Figure 11 illustrates the mechanism for H_2 production using TiO_2 (001) facet as a model with Pt nanodots and the Pt/PtO phase-juncted nanodots. Under simulated solar light, the electrons are generated from valence band (VB) of TiO_2 to conduction band (CB), which further transfer to the

highly dispersed ultra-small phase-juncted Pt/PtO hybrid nanodots and proceed the reduction of H^+ to H_2 on the activity centers of the Pt/PtO nanodots, thus facilitating the separation of photogenerated electrons and holes. Further, the coexistence of Pt^0 and Pt^{2+} in the Pt/PtO hybrid nanodots can increase the active sites and the PtO can suppress the reverse reaction of H_2 evolution. For LPC-P-TiO_2-Pt0.18, the oxidized Pt^{2+} species suppress the undesirable hydrogen back reaction comparing to LPC-P-TiO_2-Pt0.37 without Pt^{2+} species, resulting in the highly enhanced H_2 production. The phase junction formed between Pt and PtO can improve the utilization of the photogenerated electrons. In addition, the interconnected meso-macroporous TiO_2 is also helpful for light harvesting [53-56]. The synergy of these functions makes LPC-P-TiO_2-Pt0.18 with metallic Pt^0 and oxidized Pt^{2+} in the phase-juncted Pt/PtO hybrid nanodots exhibit the highest H_2 production of 65 mmol g^{-1} in 5 hours and a very stable cyclability.

4. Conclusion

A NaOH modifying TiO_2 strategy has been conducted on the deposition of Pt/PtO phase-junction in the interconnected macroporous TiO_2 with inner-particle mesoporosity from the biomolecular self-assembly mediated method for photocatalytic H_2 production. This NaOH modification process can result in not only the well deposited of phase-juncted Pt/PtO hybrid nanodots but also small size Pt/PtO nanodots in the as-prepared hierarchically porous TiO_2. After loaded with the phase-juncted Pt/PtO hybrid nanodots, the obtained LPC-P-TiO_2-Pt0.18 exhibits the H_2 production rate of 13 mmol g^{-1} h^{-1} and excellent cyclability. The excellent H_2 production performance of LPC-P-TiO_2-Pt0.18 can be attributed to the following factors: (i) most importantly, the existence of Pt^0 in Pt/PtO hybrid nanodots ensuring electron separation and migration and Pt^{2+} in

Pt/PtO hybrid nanodots providing extra photocatalytic activity sites and suppressing the H_2 oxidation; (ii) the well dispersity of Pt/PtO hybrid nanodots providing enough active sites for H_2 production; (iii) the high BET surface area from inner-particle mesopores, macropores and small TiO_2 crystallites providing deep path lengths for light harvesting in such a unique hierarchically interconnected meso-macroporous network. Our findings here may shed some light on developing and designing materials from other pollen coats for various high efficient applications such as photocatalysis, photoelectrochemistry, full cells, gas-sensing, lithium batteries and so on.

Acknowledgements

B. L. Su acknowledges the Chinese Central Government for an "Expert of the State" position in the Program of the "Thousand Talents". Y. Li acknowledges Hubei Provincial Department of Education for the "Chutian Scholar" program. This work is supported by the National Key Research and Development Program of China (2016YFA0202602), Program for Changjiang Scholars and Innovative Research Team in University (IRT_15R52), International Science & Technology Cooperation Program of China (2015DFE52870), National Natural Science Foundation of China (51502225) and the Fundamental Research Funds for the Central Universities (WUT: 2016Ⅲ029). Z. Y. Hu and G. Van Tendeloo acknowledge support from the EC Framework 7 program ESTEEM2 (Reference 312483).

References

1. Reece, S. Y.; Hamel, Sung, J. A. K.; Jarvi, T. D.; Esswein, A.; Pijpers, J. J. J.; Nocera, D. G. Wireless Solar Water Splitting Using Silicon-based Semiconductors and Earth-abundant Catalysts. *Science* **2011**, 334, 645-648.

2.Yang, J.; Wang, D.; Han, H.; Li, C. Roles of Cocatalysts in Photocatalysis and Photoelectrocatalysis. *Accounts Chem. Res.* **2013**, 46, 1900-1909.

3. Ran, J.; Zhang, J.; Yu, J. G.; Jaroniec, M.; Qiao, S. Z. Earth-abundant Cocatalysts for Semiconductor-based Photocatalytic Water Splitting. *Chem. Soc. Rev.* **2014**, 43, 7787-7812.

4. Wu, M.; Jin, J.; Liu, J.; Deng, Z.; Li, Y.; Deparis, O.; Su, B. L. High Photocatalytic Activity Enhancement of Titania Inverse Opal Films by Slow Photon Effect Induced Strong Light Absorption. *J. Mater. Chem. A* **2013**, 1, 15491-15500.

5. Wu, M.; Liu, J.; Jin, J.; Wang, C.; Huang, S. Z.; Deng, Z.; Li, Y.; Su, B. L. Probing Significant Light Absorption Enhancement of Titania Inverse Opal Films for Highly Exalted Photocatalytic Degradation of Dye Pollutants. *Appl. Catal. B: Environ.* **2014**, 150, 411-420.

6. Trasatti, S. Work Function, Eelectronegativity, and Electrochemical Behaviour of Metals: III. Electrolytic Hydrogen Evolution in Acid Solutions. *J. Electroanal. Chem. Interf.* **1972**, 39, 163-184.

7. Yu, J. G.; Qi, L.; Jaroniec, M. Hydrogen Production by Photocatalytic Water Splitting over Pt/TiO_2 Nanosheets with Exposed (001) Facets. *J. Phys. Chem. C* **2010**, 114, 13118-13125.

8. Yu, J. G.; Hai, Y.; Cheng, B. Enhanced Photocatalytic H_2-production Activity of TiO_2 by $Ni(OH)_2$ Cluster Modification. *J. Phys. Chem. C* **2011**, 115, 4953-4958.

9. Wang, F. C.; Wang, C. H.; Liu, C. W.; Chao, J. H.; Lin, C. H. Effect of Pt Loading Order on Photocatalytic Activity of Pt/TiO_2 Nanofiber in Generation of H_2 from Neat Ethanol. *J. Phys. Chem. C* **2009**, 113, 13832-13840.

10. Agegnehu, A. K.; Pan, C. J.; Rick, J.; Lee, J. F.; Su, W. N.; Hwang, B. J. Enhanced Hydrogen Generation by Eocatalytic Ni and NiO Nanoparticles Loaded on Graphene Oxide Sheets. *J. Mater. Chem.* **2012**, 22, 13849-13854.

11. Hou, Y.; Laursen, A. B.; Zhang, J.; Zhang, G.; Zhu, Y.; Wang, X.; Dahl, S.; Chorkendorff, I. Layered Nanojunctions for Hydrogen-Evolution Catalysis. *Angew. Chem. Int. Edit.* **2013**, 52, 3621-3625.

12. Lin, H. Y.; Yang, H. C.; Wang, W. L. Synthesis of Mesoporous Nb_2O_5 Photocatalysts with Pt, Au, Cu and NiO Cocatalyst for Water Splitting. *Catal. Today* **2011**, 174, 106-113.

13. Seo, S. W.; Park, S.; Jeong, H.Y.; Kim, S. H.; Sim, U.; Lee, C. W.; Nam, K. T.; Hong, K. S. Enhanced Performance of $NaTaO_3$ Using Molecular Co-catalyst $[Mo_3S_4]^{4+}$ for Water Splitting into H_2 and O_2. *Chem. Commun.* **2012**, 48, 10452-10454.

14. Yu, J. G.; Ran, J.; Facile Preparation and Enhanced Photocatalytic H_2-production Activity of $Cu(OH)_2$ Cluster Modified TiO_2. *Energ. Environ. Sci.* **2011**, 4, 1364-1371.

15. Mizukoshi, Y.; Makise, Y.; Shuto, T.; Hu, J. W.; Tominaga, A.; Shironita, S.; Tanabe, S. J. Immobilization of Noble Metal Nanoparticles on the Surface of TiO_2 by the Sonochemical Method: Photocatalytic Production of Hydrogen Form an Aqueous Solution of Ethanol. *Ultroson. Sonochem.* **2007**, 242, 387-392.

16. Puskelova, J.; Baia, L.; Vulpoi, A.; Baia, M.; Antoniadou, M.; Dracopoulos, V.; Stathatos, E.; Gabor, K.; Pap, Z.; Danciu, V.; Lianos, P. Photocatalytic Hydrogen Production Using TiO_2-Pt Aerogels. *Chem. Eng. J.* **2014**, 242, 96-101.

17. Serrano, D. P.; Calleja, G.; Pizarro, P.; Gálvez, P. Enhanced Photocatalytic Hydrogen Production by Improving the Pt Dispersity over Mesostructured TiO_2. *Int. J. Hydrogen Energ.* **2014**, 39, 4812-4819.

18. Li, Y. H.; Xing, J.; Chen, Z. J.; Li, Z.; Tian, F.; Zheng, L. R.; Wang, H. F.; Hu, P.; Zhao, H. J.; Yang, H. G. Unidirectional Suppression of Hydrogen Oxidation on Oxidized Platinum Clusters. *Nat. Commun.* **2013**, 4, 2500.

19. Xing, J.; Jiang, H. B.; Chen, J. F.; Li, Y. H.; Wu, L.; Yang, S.; Zheng, L. R.; Wang, H. F.; Hu, P.; Zhao, H. J.; Yang, H. G. Active Sites on Hydrogen Evolution Photocatalyst. *J. Mater. Chem. A.* **2013**, 1, 15258-15264.

20. Lian, Z. C.; Wang, W. C.; Li, G. S.; Tian, F. H.; Schanze, K. S.; Li, H. X. Pt-Enhanced Mesoporous Ti^{3+}/TiO_2 with Rapid Bulk to Surface Electron Transfer for Photocatalytic Hydrogen Evolution. *ACS Appl. Mater. Interfaces.* **2017**, 9, 16960-16967.

21. Lin, Z. Y.; Li, L. H.; Yu, L. L.; Yang, G. W. Modifying Photocatalyst for Solar Hydrogen Evolution Based on the Electron Behavior. *J. Mater. Chem. A.* **2017**, 5, 5235-5259.

22. Zhang, J.; Xu, Q.; Feng, Z. C.; Li, M. J.; Li, C. Importance of the Relationship between Surface Phases and Photocatalytic Activity of TiO_2. *Angew. Chem. Int. Edit.* **2008**, 47, 1766-1769.

23. Xu, Q.; Ma, Y.; Zhang, J.; Wang, X. L.; Feng, Z. C.; Li, C.; Enhancing Hydrogen Production Activity and Suppressing CO Formation from Photocatalytic Biomass Reforming on Pt/TiO_2 by Optimizing Anatase-rutile Phase Structure. *J. Catal.* **2011**, 278, 329-335.

24. Hu, Y.; Song, X.; Jiang, S. M.; Wei, C. H. Enhanced Photocatalytic Activity of Pt-doped TiO_2 for NO_x Oxidation both under UV and Visible Light Irradiation: A Synergistic Effect of Llattice Pt^{4+} and Surface PtO. *Chem. Enginer.* **2015**, 274, 102-112.

25. Wu, Z. B.; Sheng, Z. Y.; Liu, Y.; Wang, H. Q.; Mo, J. S.; Deactivation Mechanism of PtO_x/TiO_2 Photocatalyst towards the Oxidation of NO in Gas Phase. *J. Hazard. Mater.* **2011**, 185, 1053-1058.

26. Huang, C. H.; Wang, I. K.; Lin, Y. M.; Tseng, Y. H.; Lu, C. M. Visible Light Photocatalytic Degradation of Nitric Oxides on PtO_x-modified TiO_2 via Sol-gel and Impregnation Method. *J. Mol. Catal. A: Chem.* **2010**, 316, 163-170.

27. Herrmann, J. M.; Disdier, J.; Pichat, P., Photoassisted Platinum Deposition on TiO_2 Powder Using Various Platinum Complexes. *J. Phys. Chem.* **1986**, 90, 6028-6034.

28. Naldonia, A.; D'Arienzo, M.; Altomare, M.; Marelli, M.; Scotti, R.; Morazzoni, F.; Selli, E.; Santo, V. D. Pt and Au/TiO_2 Photocatalysts for Methanol Reforming: Role of Metal Nanoparticles in Tuning Charge Trapping Properties and Photoefficiency. *Appl. Catal. B Environ.* **2013**, 130, 239-248

29. Lin, C. H.; Chao, J. H.; Liu, C. H.; Chang, J. C.; Wang, F. C. Effect of Calcination Temperature on the Structure of a Pt/TiO_2 (B) Nanofiber and Its Photocatalytic Activity in Generating H_2. *Langmuir*. **2008**, 24, 9907-9915

30. Ni, M.; Leung, M. K. H.; Leung, D. Y. C.; Sumathy, K. A Review and Recent Developments in Photocatalytic Water-splitting Using TiO_2 for Hydrogen Production. *Renew. Sust. Energ. Rev.* **2007**, 11, 401-425.

31. Yang, J. H.; Wang, D.; H. Han, X.; Li, C. Roles of Cocatalysts in Photocatalysis and Photoelectrocatalysis. *Accounts Chem. Res.* **2013**, 46, 1900-1909.

32. Li, X.; Chen, Y.; Zhou, L.; Mai, Y. W.; Huang, H. Exceptional Electrochemical Performance of Porous TiO_2–carbon Nanofibers for Lithium Ion Battery Anodes. *J. Mater. Chem. A* **2014**, 2, 3875-3880.

33. Zhai, Y.; Pierre, D.; Si, R.; Deng, W.; Ferrin, P.; Nilekar, A. U.; Peng, G.; Herron, J. A.; Bell, D. C.; Saltsburg, H. Alkali-stabilized Pt-OH_x Species Catalyze Low-temperature Water-gas Shift Reactions. *Science* **2010**, 329, 1633-1636.

34. Panagiotopoulou, P.; Kondarides, D. I. Effect of Alkali Promotion of TiO_2 on theChemisorptive Properties and Water-gas Shift Activity of Supported Noble Metal Catalysts. *J. Catal.* **2009**, 267, 57-66.

35. Rondelli, M., Zwaschka, G., Krause, M., Rotzer, M. D., Hedhili, M. N., Hoger, M. P., D'Elia, V., Schweinberger, F. F., Basset, J. M., Heiz, U. Exploring the Potential of Different-sized Supported Subnano Pt Clusters as Catalysts for Wet Chemical Applications. *ACS Catal.* **2017**, 7, 4152-4162.

36. Jin, J.; Wang, C.; Ren, X. N.; Huang, S. Z.; Wu, M.; Chen, L. H.; Hasan, T.; Wang, B. J.; Li, Y.; Su, B. L. Anchoring Ultrafine Metallic and Oxidized Pt Nanoclusters on Yolk-shell TiO_2 for Unprecedentedly High Photocatalytic Hydrogen Production. *Nano Energy*. **2017**, 38, 118-126.

37. Tsuji, I.; Kato, H.; Kudo, A.; Visible-Light-Induced H_2 Evolution from an Aqueous Solution Containing Sulfide and Sulfite over a ZnS-$CuInS_2$-$AgInS_2$ Solid-Solution Photocatalyst. *Angew. Chem.* **2005**, 117, 3631-3634.

38. Haider, Z.; Kang, Y. S.; Facile Preparation of Hierarchically TiO_2 Nano Structures: Growth Mechanism and Enhanced Photocatalytic H_2 Production from Water Splitting Using Methanol as a Sacrificial Reagent. *ACS Appl. Mater. Interfaces.* **2014**, 6, 10342-10352.

39. Wang, M. J.; Shen, S. L.; Li, L.; Tang, Z. H.; Yang, J. H. Effects of Sacrificial Reagents on Photocatalytic Hydrogen Evolution over Different Photocatalysts. *J. Mater. Sci.* **2017**, 52, 5155-5164.

40. Ren, X. N.; Wu, L.; Jin, J.; Liu, J.; Hu, Z.Y.; Li, Y.; Hasan, T.; Yang, X. Y.; Van Tendeloo, G.; Su, B. L. 3D Interconnected Hierarchically Macro-mesoporous TiO_2 Networks Optimized by Biomolecular Self-assembly for High Performance Lithium Ion Batteries. *RSC Adv.* **2016**, 6, 26856-26862.

41. Jin, J.; Huang, S. Z.; Liu, J.; Li, Y.; Chen, D. S.; Wang, H. E.; Yu, Y.; Chen, L. H.; Su, B. L. Design of New Anode Materials Based on Hierarchical Three Dimensional Ordered Macro-mesoporous TiO_2 for High Performance Lithium Ion Batteries. *J. Mater. Chem. A.* **2014**, 2, 9699-9708.

42. Zhao, H.; Wu, M.; Liu, J.; Deng, Z.; Li, Y.; Su, B. L. Synergistic Promotion of Solar-driven H_2 Generation by Three-dimensionally Ordered Macroporous Structured TiO_2-Au-CdS Ternary Photocatalyst. *Appl. Catal. B: Environ.* **2016**, 184, 182-190.

43. Pan, L.; Zou, J. J.; Zhang, X.; Wang, L. Water-mediated Promotion of Dye Sensitization of TiO_2 under Visible Light. *J. Am. Chem. Soc.* **2011**, 133, 10000-10002.

44. Ohsaka, T.; Izumi, F.; Fujiki, Y. Raman Spectrum of Anatase TiO_2. *J. Raman Spectrosc.* **1978**, 7, 321-324.

45. Wang, X. C.; Zhang, X. H.; Zhong, Q. L.; Ren, B.; Tian, Z. Q. In Situ Raman Spectroscopic Studies on the Reduction Process of Various Platinum Oxides and their Effect on Methanol Oxidation. *Chinese J. Light Scattering*. **2002**, 14, 97-100.

46. Tang, H.; Xiong, M.; Qu, D.; Liu, D.; Zhang, Z.; Xie, Z.; Wei, X.; Tu, W.; Qu, D. Enhanced Supercapacitive Performance on TiO_2@C Coaxial Nano-rod Array Through a Bio-inspired Approach. *Nano Energy* **2015**, 15, 75-82.

47. Yang, D.; Sun, Y.; Tong, Z.; Tian, Y.; Li, Y.; Jiang, Z. Synthesis of Ag/TiO_2 Nanotube Heterojunction with Improved Visible-light Photocatalytic Performance Inspired by Bioadhesion. *J. Phys. Chem. C* **2015**, 119, 5827-5835.

48. Yu, J. G.; Zhao, X. J.; Zhao, Q. N. Effect of Surface Structure on Photocatalytic Activity of TiO_2 Thin Films Prepared by Sol-gel Method. *Thin Solid Films* **2000**, 379, 7-14.

49. Strataki, N.; Boukous, N.; Paloukis, F.; Neophytides, S. G.; Lianos, P. Effect of the Conditions of Platinum Deposition on Titania Nanocrystalline Films on the Efficiency of Photocatalytic Oxidation of Ethanol and Production of Hydrogen. *Photochem. Photobiol. Sci.* **2009**, 8, 639-643.

50. Yu, J. C.;Yu, J. G.; Ho, W. K.; Jiang, Z. T.; Zhang, L. Z. Effects of F-doping on the Photocatalytic Activity and Microstructures of Nanocrystalline TiO_2 Powders. *Chem. Mater.* **2002**, 14, 3808-3816

51. Zhang, W. F.; Zhang, M. S.; Yin, Z.; Chen, Q. Photoluminescence in Anatase Titanium Dioxide Nanocrystals. *Appl. Phys. B: Lasers Opt.* **2000**, 70, 261-265

52. Yu, J. G.; Yue, L.; Liu, S. W.; Huang, B. B.; Zhang, X. Y. Hydrothermal Preparation and Photocatalytic Activity of Mesoporous Au–TiO_2 Nanocomposite Microspheres. *J. Colloid Interface Sci*. **2009**, 334, 58-64.

53. Sun, M. H.; Huang, S. Z.; Chen, L. H.; Li, Y.; Yang, X. Y.; Yuan, Z. Y.; Su. B, L, Applications of Hierarchically Structured Porous Materials from Energy Storage and Conversion, Catalysis, Photocatalysis, Adsorption, Separation, and Sensing to Biomedicine. *Chem. Soc. Rev.* **2016**, 45, 3479-3563.

54. Antonelli, D. M.; Ying, J. Y.; Synthesis of Hexagonally Packed Mesoporous TiO_2 by a Modified Sol-gel method. *Angew. Chem. Int. Edit.* **1995**, 34, 2014-2017.

55. Wang, X. C.; Yu, J. C.; Ho, C.; Hou, Y. D.; Fu, X. Z. Photocatalytic Activity of a Hierarchically Macro/mesoporous Titania. *Langmuir*. **2005**, 21, 2552-2559.

56. Li, Y.; Fu, Z. Y.; Su, B. L. Hierarchically Structured Porous Materials for Energy Conversion and Storage. *Adv. Funct. Mater.* **2012**, 22, 4634-4667.

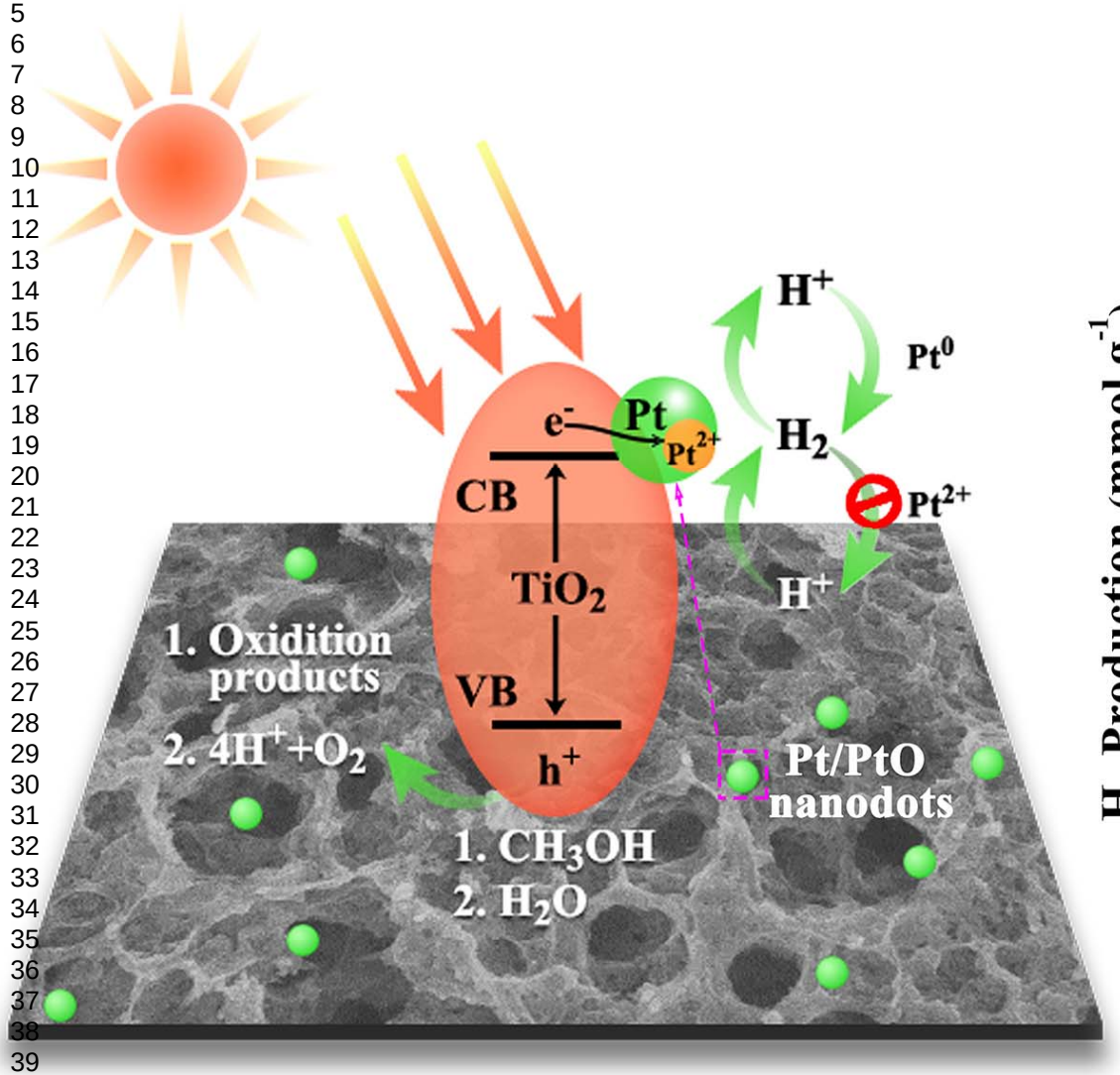
H+
Pt0
e-
Pt
Pt2+
H2
Pt2+
CB
TiO2
H+
VB
h+
1. Oxidition products
2. 4H+ +O2
Pt/PtO nanodots
1. CH3OH
2. H2O

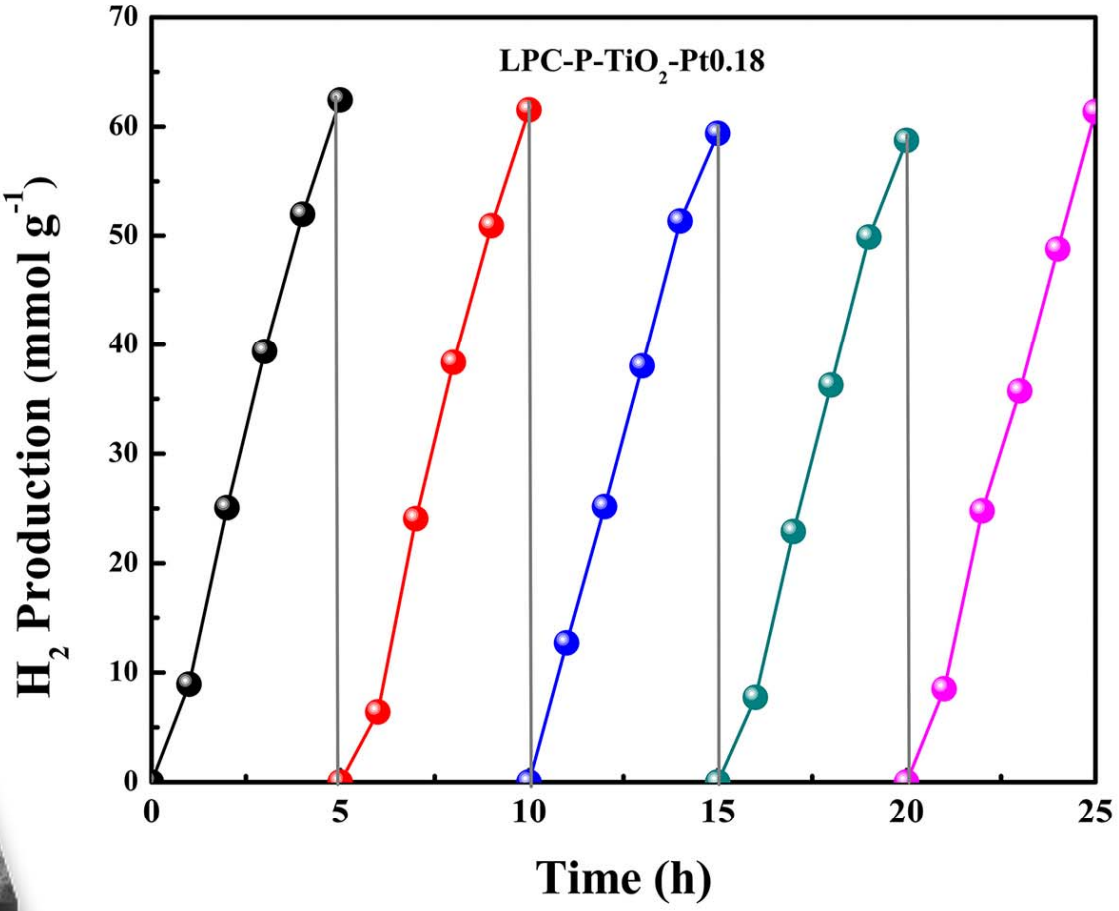
LPC-P-TiO2-Pt0.18
H2 Production (mmol g-1)
Time (h)
0
10
20
30
40
50
60
70
0
5
10
15
20
25